

Exact results of dynamical structure factor of Lieb-Liniger model

Run-Tian Li¹

Song Cheng²

E-mail: scheng@csrc.ac.cn

Yang-Yang Chen¹

E-mail: chenyy@nwu.edu.cn

Xi-Wen Guan^{3,4,5}

E-mail: xwe105@wipm.ac.cn

¹Institute of Modern Physics, Northwest University, Xi'an 710069, China

²Beijing Computational Science Research Center, Beijing 100193, China

³State Key Laboratory of Magnetic Resonance and Atomic and Molecular Physics, Wuhan Institute of Physics and Mathematics, Chinese Academy of Sciences, Wuhan 430071, China

⁴Department of Theoretical Physics, Research School of Physics and Engineering, Australian National University, Canberra ACT 0200, Australia

⁵Peng Huanwu Center for Fundamental Theory, Xi'an 710069, China

Abstract. The dynamical structure factor (DSF) represents a measure of dynamical density-density correlations in a quantum many-body system. Due to the complexity of many-body correlations and quantum fluctuations in a system of an infinitely large Hilbert space, such kind of dynamical correlations often impose a big theoretical challenge. For one dimensional (1D) quantum many-body systems, qualitative predictions of dynamical response functions are usually carried out by using the Tomonaga-Luttinger liquid (TLL) theory. In this scenario, a precise evaluation of the DSF for a 1D quantum system with arbitrary interaction strength remains a formidable task. In this paper, we use the form factor approach based on algebraic Bethe ansatz theory to calculate precisely the DSF of Lieb-Liniger model with an arbitrary interaction strength at a large scale of particle number. We find that the DSF for a system as large as 2000 particles enables us to depict precisely its line-shape from which the power-law singularity with corresponding exponents in the vicinities of spectral thresholds naturally emerge. It should be noted that, the advantage of our algorithm promises an access to the threshold behavior of dynamical correlation functions, further confirming the validity of nonlinear TLL theory besides Kitanine *et. al.* 2012 *J. Stat. Mech.* P09001. Finally we discuss a comparison of results with the results from the ABACUS method by J.-S. Caux 2009 *J. Math. Phys.* **50** 095214 as well as from the strongly coupling expansion by Brand and Cherny 2005 *Phys. Rev. A* **72** 033619.

Keywords: Lieb-Liniger model, dynamical structure factor, power-law singularity

1. Introduction

A measurement on dynamical correlations of many-body systems can be implemented by inserting into a probe, and then its scattering with constituents produces density fluctuations and tunneling rates, building on which the information one may obtain is the dynamical structure factor (DSF) and spectral function (SF) [1]. From a theoretical perspective, the DSF of a many-body system in three-dimension can be figured out by utilizing Green's function method [2]. A stark contrast to this situation is the study of dynamic correlated properties in one-dimension, wherein the reduced dimensionality and enhanced quantum fluctuation induce a non-perturbative characteristic and thus put forward new challenges. In this scenario, a variety of fruitful methods have been employed such as conformal field theory (CFT) [3], bosonization and its extension [4–8], quantum integrable theory [9, 10] and density matrix renormalization group (DMRG) method [11] etc. However, CFT and bosonization focus on the universal properties at a low energy and lack of a full-picture illustration for dynamical correlation functions. Whereas the DMRG is more suitable for the lattice systems.

Even for the arguably simplest spinless Bose gas [12], the exact evaluation of correlation functions is hard to tackle once the interaction is present, despite at a certain limit the wave function of the Tonks-Girardeau (TG) gas is known [13]. In the TG gas, the repulsive boson is reminiscent of non-interacting fermions due to the dynamic interaction, allowing a quite interesting and subtle correspondence between them. This Bose-Fermi map [13] offers a reliable access to the correlated properties of TG gases either of continuum or on a lattice, such as the DSF, one-body density matrix, one-particle dynamical correlation function, and spectral function (SF) etc [14–20]. A little bit away from the TG limit, the generalization of this map works for strongly interacting Bose gases as well, the DSF of ground state and finite temperatures of the Lieb-Liniger model are derived based on a pseudopotential Hamiltonian [21, 22]. Turning to generic interaction strength, it is totally different and difficult. Having obtained some power-law behaviour on basis of bosonization and its extension [4–8], the exact evaluation of DSF is still in great demand.

The Lieb-Liniger model describes N spinless bosons with a contact interaction in a line [12]. As one of the simplest quantum integrable models, it has been extensively studied on a variety of aspects, including thermodynamic properties and quantum criticality [23, 24], quantum interaction quench [25–31], static correlation functions [32, 33, 42] and dynamical correlation functions [21, 22, 34–41, 43, 44] etc. A quantum integrable system amenable to the Yang-Baxter equation does promise exactly solvability, however it is hardly to carry out an investigation into correlations naively from the Bethe wavefunction at a many-body level [9, 10]. On the other hand, the algebraic Bethe ansatz (ABA) provides a way to formulate a determinant representation for the form factor of a physical observable through rapidities of Bethe Ansatz

equations (BAEs) [10, 45–47]. The first successful implementation of transforming these sophisticated formulas into a useful form comes from the algebraic Bethe Ansatz-based Computation of Universal Structure factors (ABACUS) method developed by J.-S. Caux [36]. In this way, the DSF [34] and one-particle dynamic correlation [35] of ground state were calculated for a system consisting of 100 and 150 particles, respectively. However, due to the limitation of scanning algorithm and data treatment, the ABACUS method is not suitable to treat the threshold behavior of dynamical correlation functions [36].

In this scenario, we develop an efficient algorithm to compute the dynamical correlation functions of the Lieb-Liniger model with an arbitrary interaction strength by sophisticatedly counting the relevant intermediate states in the Hilbert space [39, 40]. Using this algorithm together with properly defining a set of four quantum numbers in classifying the ‘relative excitations’ over a reference state, we obtain the DSF with so far the highest accuracy and consequently its threshold behavior. In particular, the line-shape and the singular behavior of DSF close to the spectral threshold are calculated at a very large scale $N = 2000$. The emergent exponents for the edge singularity are numerically extracted and essentially confirm the validity of nonlinear Tomonaga-Luttinger (TLL) theory. We further compare our results with the ones obtained from the ABACUS [36] and other theoretical results in strongly interacting region [21]. It turns out that our algorithm offers an excellent access to the line-shape and the threshold power-law of the DSF at a significantly many-body scale, see the following discussion on Figures 2 - 9.

2. Model and DSF

The Hamiltonian of the Lieb-Liniger model reads

$$H = - \sum_{i=1}^N \frac{\partial^2}{\partial x_i^2} + 2c \sum_{i>j}^N \delta(x_i - x_j), \quad (1)$$

where $c > 0$ ($c < 0$) specifies the repulsive (attractive) interaction. Here we only consider the repulsive case. For later convenience in calculation, we define the particle density $n = N/L$ and a dimensionless interaction parameter $\gamma = c/n$. Tuning this parameter γ in the whole repulsive region, i.e. $0 \rightarrow \infty$, the ground state of system varies from quasi-condensate to TG gas. Substituting the Bethe wavefunction into the Hamiltonian, one obtains a set of transcendental equation, i.e. the Bethe ansatz equations (BAEs) [12]

$$\lambda_j + \frac{1}{L} \sum_{k=1}^N \theta(\lambda_j - \lambda_k) = \frac{2\pi}{L} I_j, \quad j = 1, \dots, N, \quad (2)$$

where $\theta(x) = 2 \arctan(x/c)$, λ_j and I_j are respectively the rapidity and its corresponding quantum number (QN). A set of $\{I_j\}$ uniquely determines a quantum state (represented by a set of $\{\lambda_j\}$), vice versa. Those QNs taking integer and half-integer depends on the parity of N , see Figure 1. The total momentum and energy of the system can be

expressed in forms of rapidities

$$P_{\{\lambda\}} = \sum_{j=1}^N \lambda_j, \quad E_{\{\lambda\}} = \sum_{j=1}^N \lambda_j^2. \quad (3)$$

It is convenient to describe the eigenstates by employing the configurations of QNs. As is sketched in Figure 1, the ground state is depicted by a Fermi sea-like distribution, over which pairs of particle-hole (p-h) excitations simply generate excited states. In principle, an arbitrary eigenstate of the Hilbert space can be accessed by manipulating a series of pairs of p-h excitations.

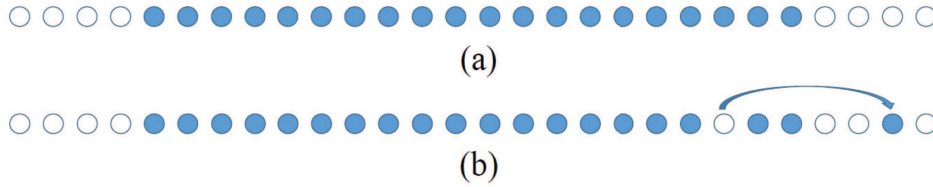


Figure 1. (a) displays the configuration of QNs in ground state, showing an analog of the Fermi sea. For a N -particle system, the ground state QNs lie between $-(N-1)/2$ and $(N-1)/2$ consecutively. (b) shows a typical example of 1-pair of particle-hole (p-h) excitation.

The dynamical structure factor [48] is defined by

$$S(k, \omega) = \frac{L}{2\pi} \int_0^L dx \int_{-\infty}^{\infty} dt e^{i(kx - \omega t)} \langle \rho(x, t) \rho(0, 0) \rangle, \quad (4)$$

where $\rho(x, t)$ is the density operator and $\langle \cdot \cdot \rangle$ means expectations taken over the state of our interest. In our realistic calculations, however, the finite temperature correlation is not carried out naively from this definition. From the macroscopic viewpoint, any equilibrium state of quantum integrable systems can be described by the thermodynamic Bethe ansatz (TBA) equations [49]. It is not an eigenstate of the system, but a mixture of microscopic states sharing the same macroscopic description of a total number $e^{\mathcal{S}}$, where \mathcal{S} is the entropy. The expectation over arbitrary one of these eigenstates gives the same result. Therefore the problem at finite temperature now is reformulated at a similar level to the ground state one. Under this circumstance, what we need is nothing but a discredited solution to the TBA. Below we call this eigenstate of our interest as reference state which can be either the ground state or a microscopic state bearing the macroscopic description for the equilibrium state at nonzero temperatures, see Figures 2 of Section Method for a simple example.

The spectral expression is obtained by inserting the completeness equality $\sum_{\{\mu\}} |\{\mu\}\rangle \langle \{\mu\}| / \langle \{\mu\} | \{\mu\} \rangle = 1$ into Equation 4

$$S(k, \omega) = L^2 \sum_{\{\mu\}} \frac{\| \langle \{\mu\} | \rho(0, 0) | \{\lambda\} \rangle \|^2}{\| \{\lambda\} \|^2 \| \{\mu\} \|^2} \delta_{k, P_{\mu, \lambda}} \delta(\omega - E_{\mu, \lambda}), \quad (5)$$

where $\delta_{m, n}$ and $\delta(x)$ are the Kronecker- and Dirac-delta functions, respectively. For simplicity, we denote $O_{\mu, \lambda} \equiv O_{\{\mu\}} - O_{\{\lambda\}}$ with $O = E$ or P . $\langle \{\mu\} | \rho(0, 0) | \{\lambda\} \rangle$ is

called *form factor* and $\|\{\nu\}\|^2$ is the norm square of eigenstate, both of which can be transformed into determinants with entries represented by rapidities [47]. The summations for intermediate states $|\{\mu\}\rangle$ is assumed to be over the whole Hilbert space, yet impossible in practice. The reasonable solution is to incorporate states with significant contributions to DSF as many as possible, before satisfying the required accuracy. The saturation is readily checked by the f -sum rule [48]

$$\int_{-\infty}^{\infty} d\omega \omega S(k, \omega) = Nk^2. \quad (6)$$

It should be noted that the DSF possess nonzero value at negative energy only if at finite temperatures, and for simplicity a normalized form of above f -sum rule is used later on.

3. Methods

It is obvious that the key to evaluating dynamical correlation functions through form factor approach is how to efficiently and quickly find the essential states in the process of navigating Hilbert space. To this end, recently we have developed an algorithm suitable for calculating various dynamical correlation functions, such as single particle Green's functions and one particle density matrix at both zero and finite temperatures [39, 40]. The idea involves two different aspects: on one side, as is explained before, the correlation function at a thermodynamic equilibrium state is transformed into a similar problem to that for ground state, i.e. expectation over an eigenstate satisfying the TBA equations; on the other side, the most relevant states for calculating the form factors of a local observable ought not to be much different to the reference state in the perspective of QNs configuration.

In light of the prospectively unified description for the reference state, one has to abandon the conventional understanding of p-h excitations shown in Figure 1. We hence define arbitrary re-distributions of QNs away from the reference state as the 'relative excitations' over it. Before moving on to the details of our algorithm, we give an example of the reference state and 'relative excitations' at finite temperatures in Figure 2. There we illustrate the reference state for a thermodynamic equilibrium state of interaction $c = 4$ and temperature $T = 3$ with a small size of $N = L = 10$. The first row corresponds to the reference state, i.e. one of the eigenstates satisfying the macroscopic descriptions of the TBA equations [49]. The following rows in the figure show the states produced by three 'relative excitations', and their classification will be discussed later on. Each arrow clearly marks the direction and step-length of the 'relative' p-h excitation. The blue (white) balls stand for the positions of QNs of the particles (holes) and the orange ones indicate the particles making up 'relative excitations'. With this setting, the conventional p-h excitation is clearly a special case of the 'relative excitation'. This is demonstrated by the Figure 3, where the first row is exactly the ground state of the same system with $N = L = 10$ and interaction $c = 4$, while the rest rows show states produced by three excitations as well.

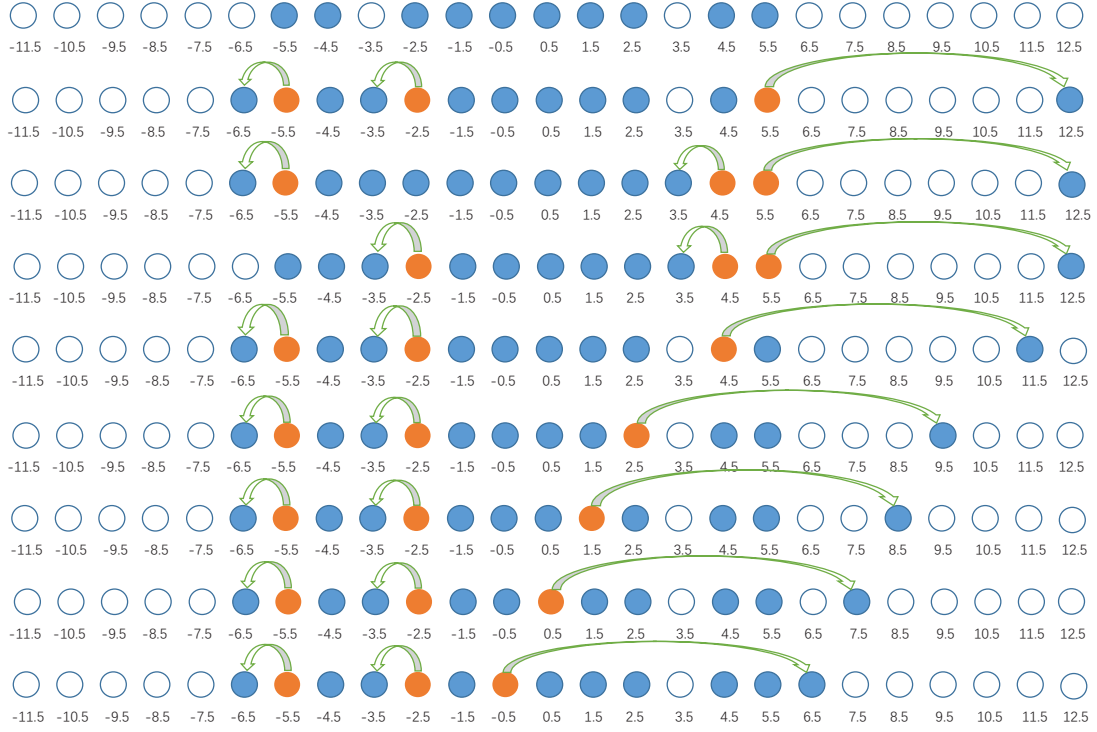


Figure 2. The first row is the reference state of the system with $N = L = 10$, interaction $c = 4$ at temperature $T = 3$. The balls mean vacancies of QNs, the blue (white) ones are occupied (un-occupied) vacancies and they stand for particles (holes). The arrow represents a ‘relative excitation’, and the orange balls indicate the particle taking part in that ‘excitation’. The following eight ‘excited states’ over this reference state belong to the set of tags $(P_m, N_p, P_l, N_l) = (5, 3, 2, 2)$. Their total contributions to the DSF is 9.4639×10^{-5} as being summarized in Table 1, and also Figure 4.

Let us first consider how to classify the excited states over a reference state. For this purpose, we introduce a set of four tags (P_m, N_p, P_l, N_l) . They are four non-negative integers, $P_m = k * L/2\pi$ is employed to specify the value of momentum of an excited state, N_p is the number of particles involved in relative excitations, $N_l < N_p$ is the number of particles jumping leftward, and $P_l \geq N_l$ is the sum of leftward step-length for all N_l particles in units of $2\pi/L$. They can be seen as a set of quantum numbers to describe the ‘relative excitations’ over a reference state. In this way, the Hilbert space is separated into a large number of subspaces, and one may find the most relevant states by a proper choice of the sets of tags. It should be stressed that the strategy of our navigation of states is rather different to the ABACUS [36] in several aspects. The value of momentum is chosen as the first tag, making an efficient way of counting states for computing the line-shape of dynamic correlation functions. We define the ‘relevant excitations’ and use their number N_p instead of the conventional p-h excitation number. On account of the mirror-symmetric distribution of DSF with respect to energy axis, we make use of four tags of (P_m, N_p, P_l, N_l) instead of energy as a criteria for cut-off. All these are essentially different from the counting manner in [36]. Since this partition based on sets of tags depends on the reference state, it is efficient to accelerate the

search of those relevant states that make non-negligible sum-rule weights. This method is especially efficient for finite temperature situation.

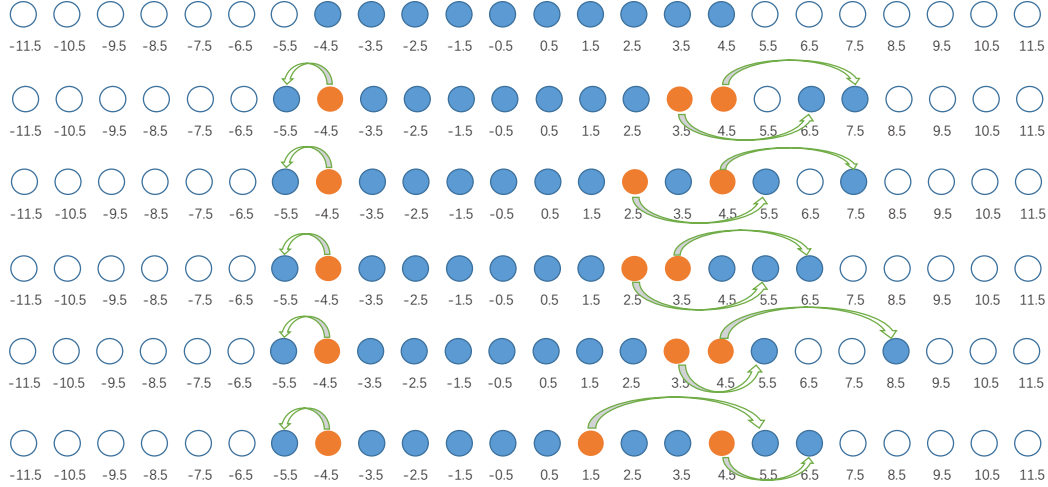


Figure 3. The first row is the ground state of a system with $N = L = 10$ and interaction $c = 4$. The following are the excited states belonging to the set of tags $(P_m, N_p, P_l, N_l) = (5, 3, 1, 1)$. Their contribution to the weights of the sum rule for the DSF is 7.7379×10^{-5} , also see the case at the ground state showing in Table 2 and Figure 5. The notations for the different color balls are the same as that in Figure 3. Obviously, the ‘relative excitations’ here reduce to the conventional p-h excitations as being shown by Figure 1.

We give an example, the eight excited states belonging to the set of tags $(P_m, N_p, P_l, N_l) = (5, 3, 2, 2)$ with respect to reference state determined by interaction $c = 4$ and temperature $T = 3$, see Figure 2. A similar example for ground state is displayed by Figure 3 with $(P_m, N_p, P_l, N_l) = (5, 3, 1, 1)$. For the sake of clarity, below we sketch the construction of the five excited states in Figure 3. There are $N_p = 3$ orange balls, one of them jump leftward with a step-length 1, and the two particles jumping rightward need to move a total sum of step-length $P_m + P_l = 6$ for compensation of the leftward excitations. Then the division of 6 into a sum of 2 positive integers as $3 + 3$, $2 + 4$ and $1 + 5$ leaves only five available arrangements. For the number of states belonging to different sets of tags, one may refer to Figure 4 and Table 1 (Figure 5 and Table 2), illustrating an example of finite temperature excitations (excitation over ground state similarly).

In order to illustrate the efficiency of our algorithm, in Figure 4 and Table 1 (Figure 5 and Table 2) we show a sample of data for calculating the DSF $S(k = k_F, \omega)$ at the finite temperature (in ground state). The temperature and interaction is set

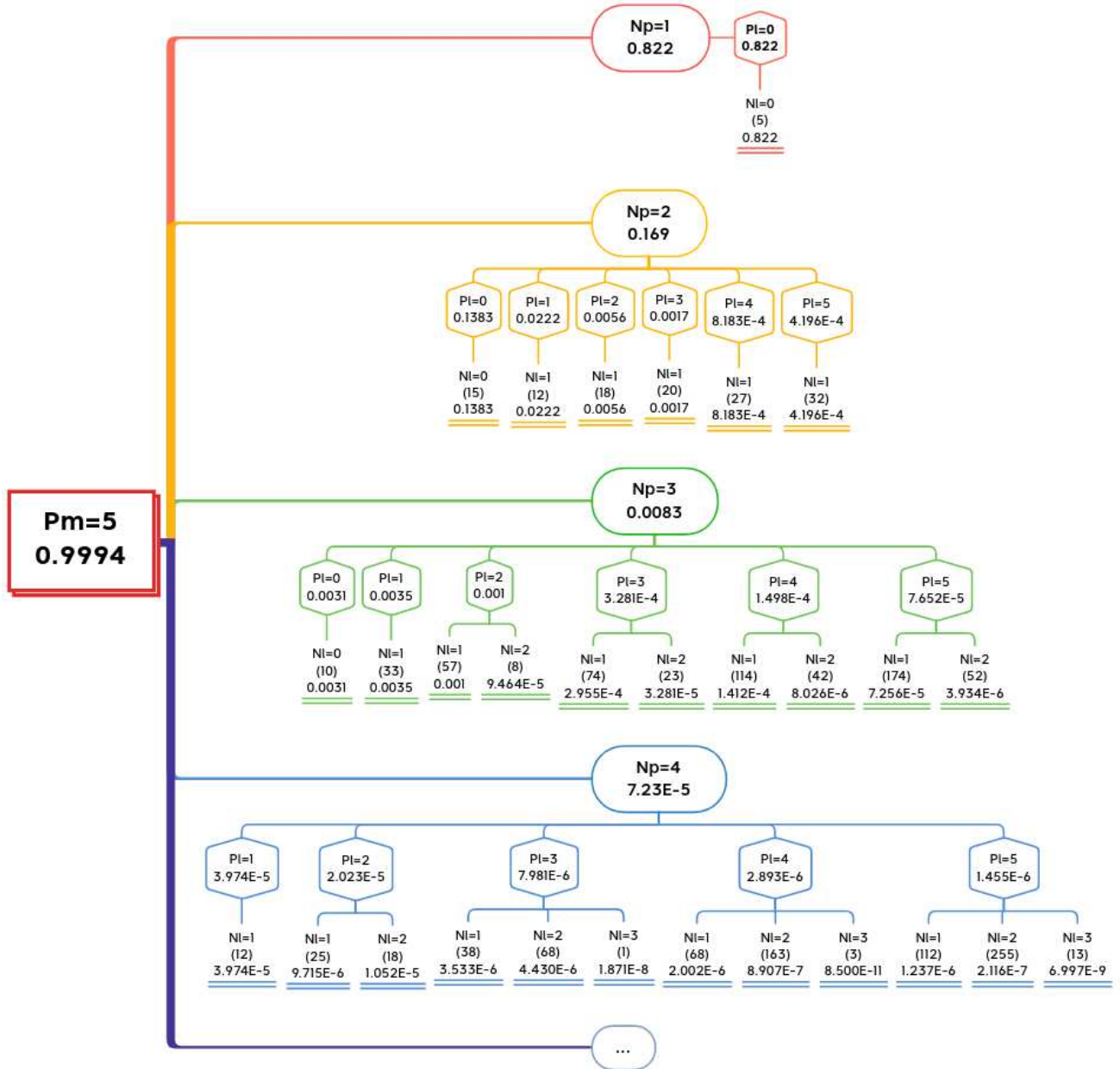


Figure 4. The sum rule weights associated with the data given in Table 2 for the DSF $S(k_F, \omega)$ at a finite temperature with $N = L = 10$, interaction $c = 4$ and temperature $T = 3$. Each set of tags (P_m, N_p, P_l, N_l) attributes to the roots of the sum rule tree. The number in the parentheses at the end root for each N_l is the number of states belonging to the set of tags. The weight of the f -sum rule of each branch is given level by level, i.e. containing a sum of all branches of next level. The eight states of tags $(5, 3, 2, 2)$ are also shown in Figure 2.

Table 1. The sum rule weights of the DSF at $k = k_F$ of the system with $N = L = 10$, interaction strength $\gamma = 4$ and temperature $T = 3$. The X-sum rule is the total spectral weights of the states under tag X, and the N_p -sum rule specifies the contributions of different pairs relative p-h excitations. The tree structure of this sample is shown in Figure 4 and the states belonging to the set of tags (5, 3, 2, 2) are demonstrated in Figure 2.

| Tags | | | | Number of States | Sum Rule | | | |
|-------|-------|----------|----------|------------------|--------------------------|-------------------------|-------------------------|-----------------|
| P_m | N_p | P_l | N_l | | N_l -sum rule | P_l -sum rule | N_p -sum rule | P_m -sum rule |
| 5 | 1 | 0 | 0 | 5 | 0.8220 | 0.8220 | 0.8220 | 0.9994 |
| 5 | 2 | 0 | 0 | 15 | 0.1383 | 0.1383 | 0.1690 | |
| 5 | 2 | 1 | 1 | 12 | 0.0222 | 0.0222 | | |
| 5 | 2 | 2 | 1 | 18 | 0.0056 | 0.0056 | | |
| 5 | 2 | 3 | 1 | 20 | 0.0017 | 0.0017 | | |
| 5 | 2 | 4 | 1 | 27 | 8.1834×10^{-4} | 8.1834×10^{-4} | | |
| 5 | 2 | 5 | 1 | 32 | 4.1960×10^{-4} | 4.1960×10^{-4} | | |
| 5 | 2 | \vdots | \vdots | \vdots | \vdots | \vdots | | |
| 5 | 3 | 0 | 0 | 10 | 0.0031 | 0.0031 | 0.0083 | |
| 5 | 3 | 1 | 1 | 33 | 0.0035 | 0.0035 | | |
| 5 | 3 | 2 | 1 | 57 | 0.0010 | 0.0010 | | |
| 5 | 3 | 2 | 2 | 8 | 9.4639×10^{-5} | | | |
| 5 | 3 | 3 | 1 | 74 | 2.9547×10^{-4} | 3.2809×10^{-4} | | |
| 5 | 3 | 3 | 2 | 23 | 3.2809×10^{-5} | | | |
| 5 | 3 | 4 | 1 | 114 | 1.4178×10^{-4} | 1.4980×10^{-4} | | |
| 5 | 3 | 4 | 2 | 42 | 8.0263×10^{-6} | | | |
| 5 | 3 | 5 | 1 | 174 | 7.2585×10^{-5} | 7.6523×10^{-5} | | |
| 5 | 3 | 5 | 2 | 52 | 3.9388×10^{-6} | | | |
| 5 | 3 | \vdots | \vdots | \vdots | \vdots | \vdots | | |
| 5 | 4 | 0 | 0 | 0 | 0 | 0 | 7.2300×10^{-5} | |
| 5 | 4 | 1 | 1 | 12 | 3.9739×10^{-5} | 3.9739×10^{-5} | | |
| 5 | 4 | 2 | 1 | 25 | 9.7145×10^{-6} | 2.0233×10^{-5} | | |
| 5 | 4 | 2 | 2 | 18 | 1.0518×10^{-5} | | | |
| 5 | 4 | 3 | 1 | 38 | 3.5330×10^{-6} | 7.9812×10^{-6} | | |
| 5 | 4 | 3 | 2 | 68 | 4.4295×10^{-6} | | | |
| 5 | 4 | 3 | 3 | 1 | 1.8712×10^{-8} | | | |
| 5 | 4 | 4 | 1 | 68 | 2.0018×10^{-6} | 2.8926×10^{-6} | | |
| 5 | 4 | 4 | 2 | 163 | 8.9070×10^{-7} | | | |
| 5 | 4 | 4 | 3 | 3 | 8.4996×10^{-11} | | | |
| 5 | 4 | 5 | 1 | 112 | 1.2367×10^{-6} | 1.4552×10^{-6} | | |
| 5 | 4 | 5 | 2 | 255 | 2.1156×10^{-7} | | | |
| 5 | 4 | 5 | 3 | 13 | 6.9973×10^{-9} | | | |
| 5 | 4 | \vdots | \vdots | \vdots | \vdots | \vdots | | |

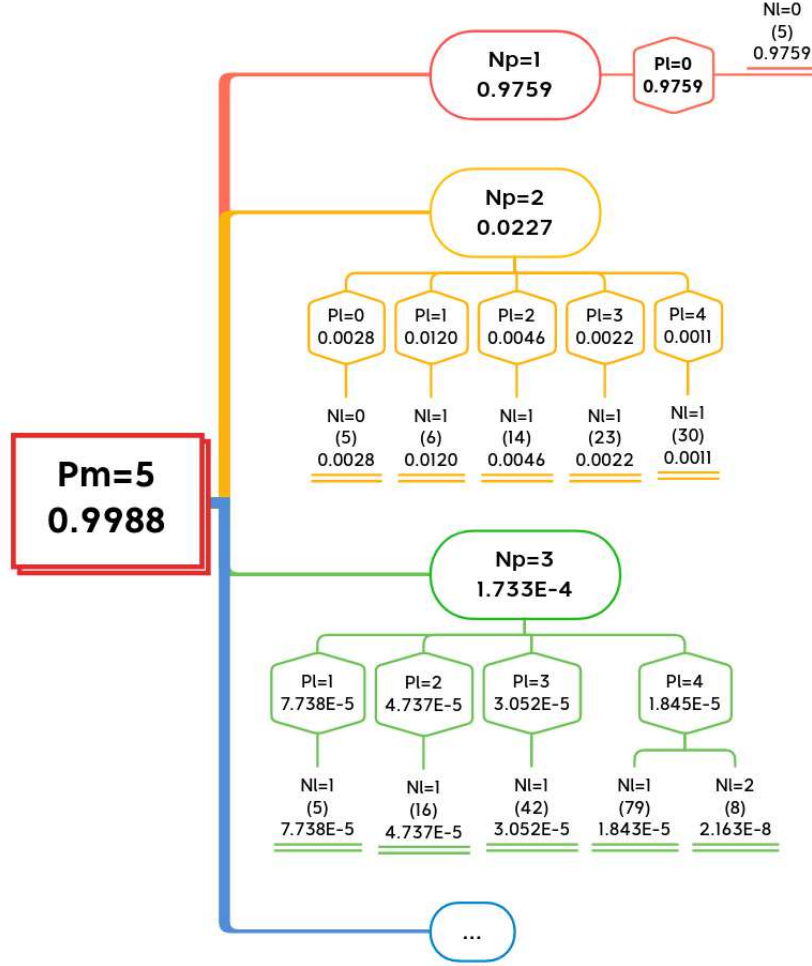


Figure 5. The sum rule weights associated with the data given in Table 3 for DSF $S(k_F, \omega)$ in the ground state of the system with $N = L = 10$ and interaction $c = 4$. Each set of tags (P_m, N_p, P_1, N_1) attributes to the roots of the sum rule tree. The number in the parentheses at the end root for each N_1 is the number of states belonging to the set of tags for the ground state. The weight of the f -sum rule of each branch is given level by level, i.e. containing a sum of all branches of next level. The eight states of tags (5, 3, 1, 1) are also shown in Figure 3.

by $T = 3$ ($T = 0$) and $c = 4$, while the system size $N = L = 10$ for the sake of a clear visibility. The tree in Figure 4 (Figure 5) obviously shows the data structure of DSF in terms of weights of the sum rule associated with the quantum numbers N_p , P_1 and N_1 , which serve as a good criterion for truncation in numerical calculations. The good saturation of the sum rule confirms the validity of our algorithm for both ground state and finite temperature environments. We would like to remark that our method works well for calculation of other correlation functions, such as one-particle dynamic correlation function at the finite temperatures [40].

Table 2. The sum rule weights of the DSF at $k = k_F$ of the system with $N = L = 10$, interaction strength $\gamma = 4$ at zero temperature. The X-sum rule is the total spectral weights of the states under tag X, and the N_p -sum rule specifies the contributions of different pairs of relative p-h excitations. The tree structure of this sample is shown in Figure 5 and the states belonging to the set of tags (5, 3, 1, 1) are demonstrated in Figure 3.

| Tags | | | | Number of States | Sum Rule | | | |
|-------|----------|----------|----------|------------------|-------------------------|-------------------------|-------------------------|-----------------|
| P_m | N_p | P_l | N_l | | N_l -sum rule | P_l -sum rule | N_p -sum rule | P_m -sum rule |
| 5 | 1 | 0 | 0 | 5 | 0.9759 | 0.9759 | 0.9759 | 0.9988 |
| 5 | 2 | 0 | 0 | 2 | 0.0028 | 0.0028 | 0.0227 | |
| 5 | 2 | 1 | 1 | 6 | 0.0120 | 0.0120 | | |
| 5 | 2 | 2 | 1 | 14 | 0.0046 | 0.0046 | | |
| 5 | 2 | 3 | 1 | 23 | 0.0022 | 0.0022 | | |
| 5 | 2 | 4 | 1 | 30 | 0.0011 | 0.0011 | | |
| 5 | 2 | \vdots | \vdots | \vdots | \vdots | \vdots | | |
| 5 | 3 | 0 | 0 | 0 | 0 | 0 | 1.7332×10^{-4} | |
| 5 | 3 | 1 | 1 | 5 | 7.7379×10^{-5} | 7.7379×10^{-5} | | |
| 5 | 3 | 2 | 1 | 16 | 4.7372×10^{-5} | 4.7372×10^{-5} | | |
| 5 | 3 | 2 | 2 | 0 | 0 | | | |
| 5 | 3 | 3 | 1 | 42 | 3.0517×10^{-5} | 3.0517×10^{-5} | | |
| 5 | 3 | 3 | 2 | 0 | 0 | | | |
| 5 | 3 | 4 | 1 | 79 | 1.8430×10^{-5} | 1.8452×10^{-5} | | |
| 5 | 3 | 4 | 2 | 8 | 2.1633×10^{-8} | | | |
| 5 | 3 | \vdots | \vdots | \vdots | \vdots | \vdots | | |
| 5 | \vdots | \vdots | \vdots | \vdots | \vdots | \vdots | | |

4. Results

Using the method explained in the above section, we demonstrate the ground state DSFs for the system with different interaction strength $\gamma = 1$ and $\gamma = 5$ in Figure 6, where the system size is $N = L = 100$. For the sake of visibility, we plot $\log_{10}(S/L)$ in momentum-energy plane, where the brighter is the color the larger is the DSF therein. There are two types of single-particle dispersion relations for this model, i.e. Lieb-I and Lieb-II. The former (latter) is produced by putting a particle (hole) outside (inside) the Fermi sea which we denote as ε_p (ε_h). It is blank below the Lieb-II excitation because there is no state bearing energy lower than a single-hole excitation. The ε_p - and ε_h -dispersion relations respectively define the upper and lower thresholds of single-particle spectra. Above ε_p , all the signals come from these states generated by multiple pairs of p-h excitations. It is obvious that the strongest signals of the DSF concentrate

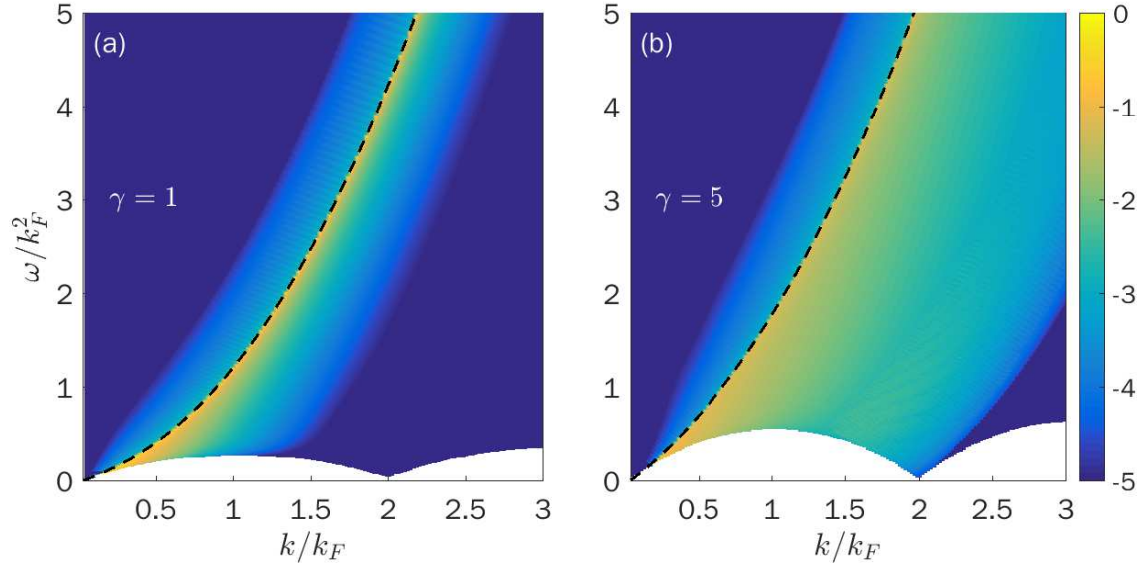


Figure 6. (a) and (b) shows the logarithmic DSF for different interaction strength $\gamma = 1$ and $\gamma = 5$, respectively. Without losing generality, we tune the interaction strength parameter c with keeping the particle density intact $n = 1$, and here the system size is $N = L = 100$. The momentum and energy are measured in units of Fermi momentum and Fermi energy, respectively. The brighter the color, the larger the DSF. The black dashed curve marks the position of Lieb-I type of dispersion relation, where the DSF diverges in thermodynamic limit.

along on $\varepsilon_p(k)$. In thermodynamic limit, a power-law divergence occurs in the vicinities of the dispersion, which will be studied in more details later. In comparison of the cases of different interactions, it is apparent that if γ vanishes eventually, then only the ε_p -dispersion survives, and the corresponding DSF finally shrinks into a δ -function; whereas the hole dispersion ε_h disappears as γ tends to zero. In another word, the interaction changes the distributions of the spectral weights of DSF, and the divergence of δ -function is replaced by a power-law singularity. To prove the validity of our results given in Figure 6, the values of f -sum rule at different momenta k are listed in Table 3.

Table 3. f -sum rule at momentum k with interaction strength $\gamma = 1$ and $\gamma = 5$, respectively. The data come from plot of Figure 6, and the f -sum rule shows the precision of our results.

| k/k_F | 0.5 | 1.0 | 1.5 | 2.0 | 2.5 | 3.0 |
|--------------|--------|--------|--------|--------|--------|--------|
| $\gamma = 1$ | 99.66% | 99.22% | 98.96% | 98.79% | 95.30% | 95.02% |
| $\gamma = 5$ | 99.74% | 99.17% | 98.22% | 96.98% | 95.73% | 94.63% |

The typical line-shapes of DSF for a given momentum $k = 0.5k_F$ of the system at different interaction strengths $\gamma = 1$ and $\gamma = 5$ are illustrated in Figures 7 (a) and 8 (a), where the system size is taken as $N = L = 2000$ in order to capture the threshold

singularity. It clearly shows that for an arbitrary γ , the signal of the DSF mainly spreads in a certain region between the particle and hole dispersion lines. In particular, a sharp peak in the vicinity of the dispersion ε_p remarkably emerges and it suddenly decreases once the frequency goes over the dispersion line. In the spectral continuum between ε_h and ε_p , the most weights of the DSF come from states generated by the 1-pair of p-h excitation. In the vicinities of the two spectral thresholds, those states are in charge of the power-law behavior as well. As being mentioned, the DSF at a given momentum is a δ -function in non-interacting limit, while a flat plateau shows in TG limit. A comparison of Figures 7 (a) and 8 (a) exemplifies the role of interaction in forming the dynamical correlation functions, showing the evolution of line-shapes between the above two limiting situations.

In Figures 7 (b) & (c) and 8 (b) & (c), the behavior of the DSF in the vicinities of spectral thresholds is demonstrated, showing a power law as following

$$S(k, \omega) \sim \text{const} + |\omega - \varepsilon_{p,h}|^{\mu_{p,h}}. \quad (7)$$

Here $\mu_{p,h}$ stand for the exponents of the DSF in the vicinities of the Lieb-I and -II dispersion lines respectively. The exponent μ (μ_h) is negative (or positive) and

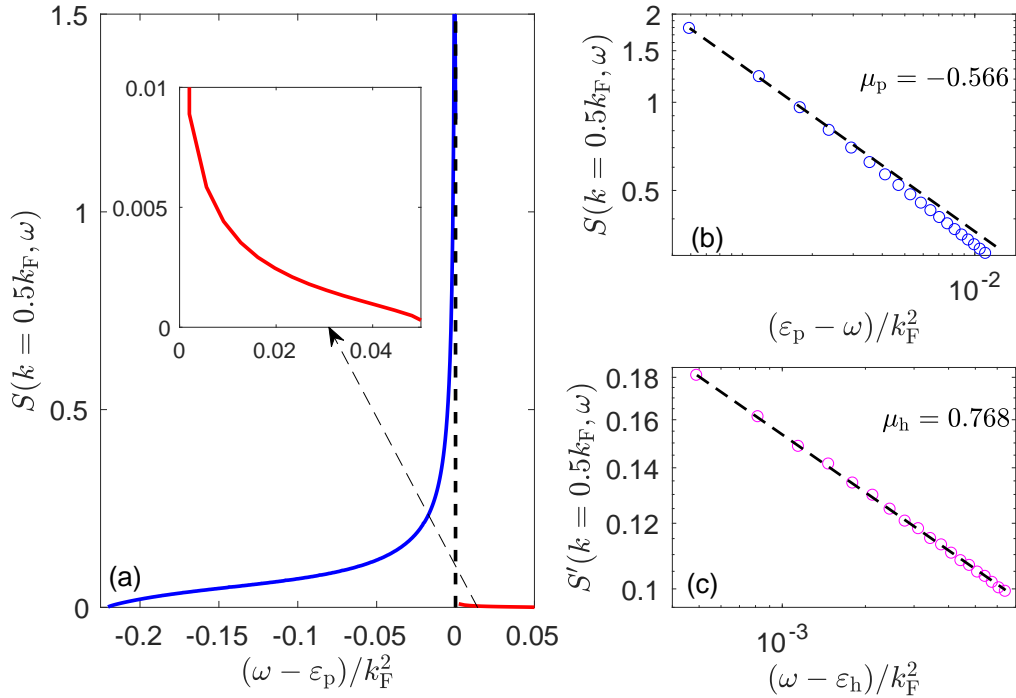


Figure 7. (a) shows the lines shape of $S(k, \omega)$ vs ω with excited momentum $k = 0.5k_F$ and interaction strength $\gamma = 1$. The system size is as large as $N = L = 2000$. The inset shows the rightward of the peak, i.e. the tail of the DSF with large frequency. (b) and (c) respectively show the power-law behavior of the DSF close to upper and lower spectral thresholds by the log-log coordinate. The dotted and dashed lines correspond to the original data of calculation and the extracted exponents, respectively. By utilizing the nonlinear Tomonaga-Luttinger liquid theory, the exponents on $\varepsilon_{p,h}$ are -0.567 and 0.810 , agreeing well with our results -0.566 and 0.768 , respectively.

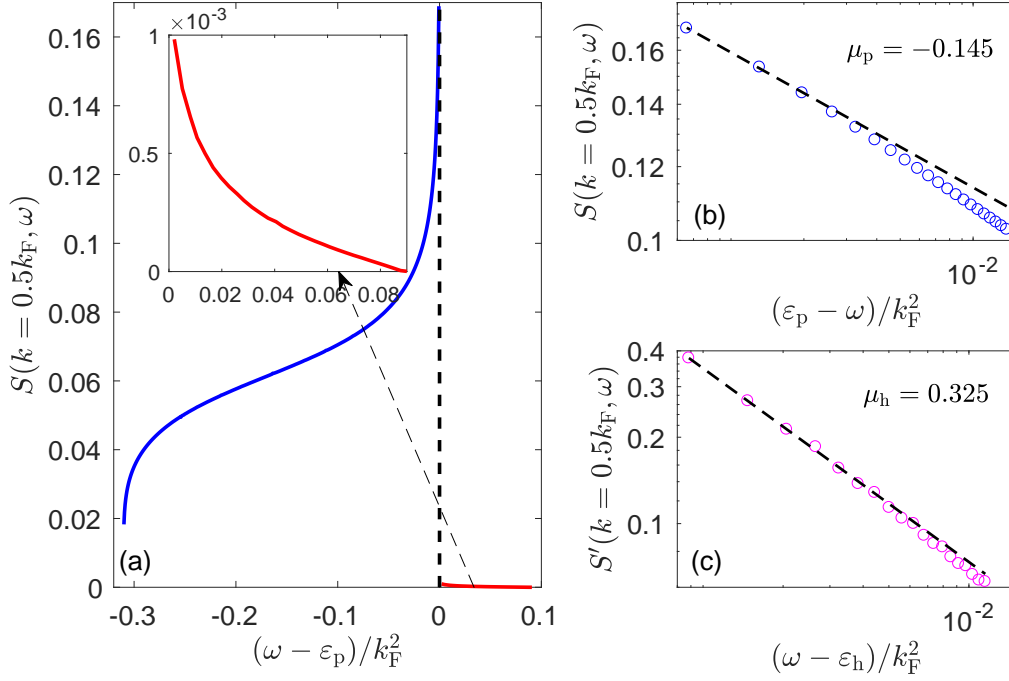


Figure 8. (a) shows the lines shape of $S(k, \omega)$ vs ω with excited momentum $k = 0.5k_F$ and interaction strength $\gamma = 1$. The system size is as large as $N = L = 2000$. The inset shows the rightward of the peak, i.e. the tail of the DSF with large frequency. (b) and (c) respectively show the power-law behavior of the DSF close to upper and lower spectral thresholds by the log-log coordinate. The dotted and dashed lines correspond to the original data of calculation and the extracted exponents, respectively. By utilizing the nonlinear Tomonaga-Luttinger liquid theory, the exponents on $\varepsilon_{p,h}$ are -0.177 and 0.202 , agreeing well with our results -0.145 and 0.325 , respectively.

essentially depends on k and γ [8, 50–52]. Such a singularity is caused by the collective behaviour of the interacting particles. This phenomenon is a reminiscence of Fermi edge singularity (FES) firstly observed in 3D electronic systems [53]. A simple explanation underlies FES is that an excitation of a deep electron leaves behind a hole in valence band, and this deep hole scatters the electrons in conduction band, resulting in a power-law for spectral function on the threshold [4, 53]. This puzzle can be figured out by recasting it into a problem of single impurity moving in a cloud of non-interacting electrons. On account of interaction effect in 1D, here it evolves into the situation of an impurity in TLL [4, 54]. More specific to the interacting fermions in 1D, one sees that a moving hole in the Fermi sea scatters the low-lying excited particles. The physics of this phenomenon is captured by projecting the system into a three-subbands model, where two subbands are for the low-lying excitations close to both Fermi points and one for the moving hole. The interaction between the TLL and impurity can be removed by a unitary transformation which is dependent of the phase shifts of excited particles. Eventually the edge singularity can be extracted by a standard treatment of bosonization [4, 8, 54]. The same property for bosonic system and spin chains can be figured out by mapping that system into fermions through the Jordan-

Wigner transformation. In the method of nonlinear TLL, this power-law behavior have been found for both DSF and SF in a variety of 1D quantum systems [8, 50, 51, 55–59].

For a good visibility, we use a log-log coordinate in Figures 7 (b) & (c) and 8 (b) & (c), and the slopes extracted from our data are represented by the black dashed lines. It should be noted that the treatments of the DSFs for the vicinities of upper and lower thresholds are different. In the vicinity of $\varepsilon_p(k)$, the DSF diverges, hence it is safe to ignore the ‘const’ there. For the threshold $\varepsilon_h(k)$, the derivative of the DSF with respect to ω , i.e. $S'(k, \omega)$ is employed in order to rule out the influence of the constant background value. As being shown in Figures 7 (b) & (c) and 8 (b) & (c), the exponents for $\gamma = 1$ ($\gamma = 5$) are respectively given by -0.566 and 0.768 (-0.145 and 0.325), in agreement with the nonlinear TLL predictions -0.567 and 0.810 (-0.177 and 0.202) [50, 52]. The advantage of our algorithm is that the quantum numbers P_m and N_p , P_l and N_l well sort of states in terms of sum rule weights and they serve as a good criterion for making a suitable truncation in the navigation of Hilbert space. The convenient fixing excited momentum k is especially helpful in studying the line-shape of dynamical correlation functions

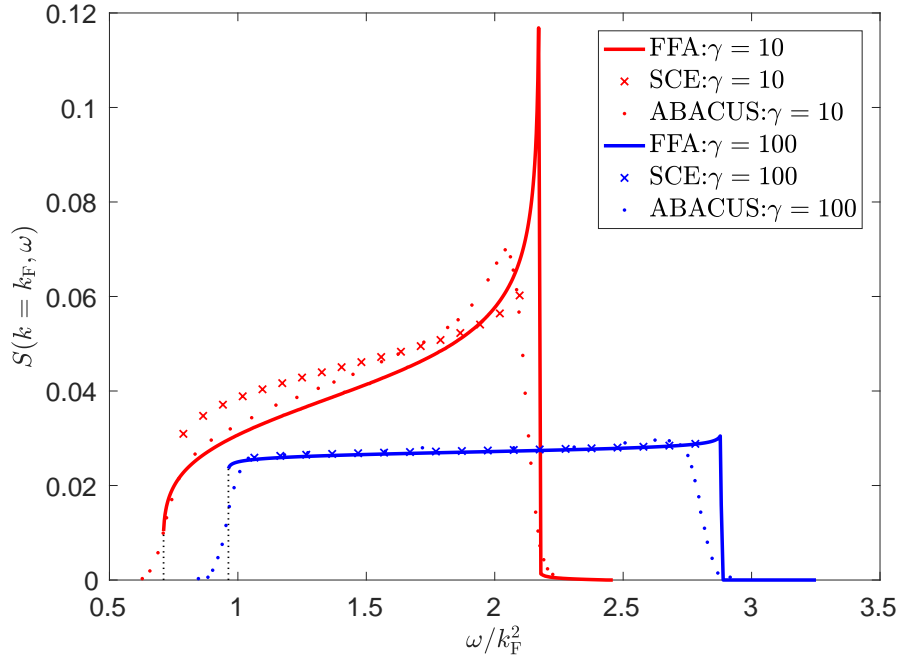


Figure 9. The comparison of line-shapes for $S(k_F, \omega)$ obtained from ABACUS, our form factor approach (FFA) and strongly coupling expansion (SCE). The line, dots and crosses denote the results of FFA, ABACUS and SCE respectively, while the red and blue indicate the cases of interaction strength $\gamma = 10$ and $\gamma = 100$ respectively. The vertical black dashed lines in the left end of DSF specify the Lieb-II excitation energy, below which energy the DSF should vanish. Note that SCE validates only in the continuum between ε_h and ε_p . The system size to implement FFA is set as $N = L = 1000$, and results of ABACUS come from [34] with system size $N = L = 100$.

Our algorithm is quite different from the one developed in ABACUS [36]. In Figure 9 we compare results from our form factor approach (FFA) with the that obtained

from the strongly coupling expansion (SCE) method [21] and the ABACUS [34]. The SCE is only valid in the continuum between ε_h and ε_p , and expressed as following

$$\frac{S(k, \omega)}{L} = \frac{1}{4\pi k} \left(1 + \frac{8}{\gamma}\right) + \frac{1}{2\pi\gamma k_F} \ln \frac{\omega - \varepsilon_h^2}{\varepsilon_p^2 - \omega^2} + o\left(\frac{1}{\gamma^2}\right). \quad (8)$$

In the case of $\gamma = 100$, we observe that the three results in the continuum agree with each other, however, the agreements break down in the neighborhood of thresholds. This is partly because the limitation of ABACUS algorithm and thus a small system size here $N = L = 100$, and partly because a Gaussian is used to replace the Dirac-delta function in Equation 5. The latter is to smoothen the line-shape of dynamical correlation functions in the continuum when the system size is not large enough, nevertheless at the cost of blurring their threshold behavior [60]. For the case of $\gamma = 10$, as being expected, the performance of SCE is not good, whereas the results obtained from the ABACUS and that FFA basically agree with each other except in the vicinities of spectral thresholds.

5. Conclusion

We have introduced ‘relative excitations’ characterized by the quantum numbers N_p , P_l and N_l for our new algorithm to precisely calculate the dynamical correlation functions over an arbitrary state, i.e. either the ground state or the equilibrium states at finite temperatures. In our algorithm, it is easy to fix the excited momentum by the tag of quantum number P_m , so is the truncation of the evaluation with the help of quantum numbers N_p , P_l and N_l . Such a set of tags is very convenient to implement the calculation of dynamical correlation functions at a very large scale. Using this newly developed algorithm, we have presented the exact DSF of Lieb-Liniger model by means of form factor approach. We have explicitly obtained the power-law behavior of the DSF in the vicinities of single-particle spectral thresholds at a many-body level $N = 2000$. While the typical line-shape of $S(k, \omega)$ vs ω with given momentum has been demonstrated as well. On top of the full picture of line-shape, the corresponding exponents of edge singularity are extracted and further confirm the validity of nonlinear TLL theory besides [52]. Furthermore, we have compared our results with that obtained from the ABACUS and strongly coupling expansion SCE, and observed their discrepancies from our calculations and the nonlinear TLL theory, indicating that the Gaussian used in the ABACUS is unnecessary at a large system size. Our work offers a reliable approach to the correlation properties merely emergent in thermodynamic limit, and manifests the form factor approach itself as a benchmark of the state-of-art ultra-cold atom experiments in near future [61–63].

Acknowledgments

This work is supported by National Natural Science Foundation of China Grants Nos. 12104372, 12047511, 12134015, 11874393 and 12121004. SC acknowledges the computational resources from the Beijing Computational Science Research Center.

Appendix

Form factor

Here we present the necessary formulas for our numeric evaluation. The theoretical derivation of the form factor was given in [47]. By using form factor, the DSF is expressed in terms of rapidities as following

$$S(k, \omega) = L^2 \sum_{\{\mu\}} k^2 \prod_{j,k}^N \frac{\lambda_{jk}^2 + c^2}{(\mu_j - \lambda_k)^2} \frac{\|\det_N U(\{\mu\}, \{\lambda\})\|^2}{\|V_p^+ - V_p^-\|^2 \|\{\mu\}\|^2 \|\{\lambda\}\|^2} \delta_{k,P_{\mu,\lambda}} \delta(\omega - E_{\mu,\lambda}) \quad (\text{A.1})$$

where for simplicity we denote $\nu_{jk} \equiv \nu_j - \nu_k$, and $O_{\mu,\lambda} \equiv O_\mu - O_\lambda$ with $O = E$ or P . In above equation, p can be any integer $p \in [1, N]$, and we usually set it as N . The norm square of eigenstate $\|\{\nu\}\|^2$ reads

$$\|\{\nu\}\|^2 = c^N \prod_{j>k}^N \frac{\nu_{jk}^2 + c^2}{\nu_{jk}^2} \det_N \mathcal{G}(\{\nu\}) \quad (\text{A.2})$$

where the entry of matrix $\mathcal{G}(\{\nu\})$ is expressed by

$$\mathcal{G}_{jk}(\{\nu\}) = \delta_{jk} \left[L + \sum_{a=1}^N K(\lambda_j, \lambda_a) \right] - K(\lambda_j, \lambda_k) \quad (\text{A.3})$$

with kernel function

$$K(x, y) = \frac{2c}{(x - y)^2 + c^2}. \quad (\text{A.4})$$

The matrix V^\pm and $U(\{\mu\}, \{\lambda\})$ are respectively defined by following entries

$$V_j^\pm = \frac{\prod_{a=1}^{N-1} (\mu_a - \lambda_j \pm ic)}{\prod_{b=1}^N (\lambda_b - \lambda_j \pm ic)}, \quad (\text{A.5})$$

and

$$U_{jk}(\{\mu\}, \{\lambda\}) = \delta_{jk} \frac{(V_j^+ - V_j^-)}{i} + \frac{\prod_{a=1}^{N-1} (\mu_a - \lambda_j)}{\prod_{b \neq j}^N (\lambda_b - \lambda_j)} [K(\lambda_j, \lambda_k) - K(\lambda_N, \lambda_k)]. \quad (\text{A.6})$$

Exponents determined by the nonlinear Tomonaga-Luttinger liquid theory

We explain how to carry out the calculation of exponents by using the nonlinear Tomonaga-Luttinger liquid theory. The interested readers may refer to [50] for more details.

$$S(k, \omega) \sim \text{const} + |\omega - \varepsilon_{p,h}|^{\mu_{p,h}}. \quad (\text{A.7})$$

In order to obtain above exponents, we need to solve two integral equations. One is the shift function [10]

$$F_B(\nu|\lambda) = \frac{\pi + \theta(\nu - \lambda)}{2\pi} + \frac{1}{2\pi} \int_{-q}^q d\mu K(\nu, \mu) F_B(\mu|\lambda) \quad (\text{A.8})$$

where $\theta(x) = 2 \arctan(x/c)$ and $K(x, y)$ is defined by equation (A.4). Note that $q > 0$ is the cut-off of rapidity for ground state in thermodynamic limit. The other one is for the

dressed momentum, i.e. the change of total momentum when adding a particle (hole) with rapidity $\lambda > q$ ($|\lambda| < q$) to the ground state. This change $k(\lambda)$ is expressed by

$$k(\lambda) = \pm \left(\lambda - \pi n + \int_{-q}^q d\nu \theta(\lambda - \nu) \rho(\nu) \right) \quad (\text{A.9})$$

where \pm is to specify adding a particle or hole and $\rho(x)$ is the distribution of rapidity in thermodynamic limit, governed by following integral equation

$$\rho(\lambda) = \frac{1}{2\pi} + \frac{1}{2\pi} \int_{-q}^q d\mu K(\lambda, \mu) \rho(\mu). \quad (\text{A.10})$$

The exponent reads

$$\mu = \frac{1}{2} \left(\frac{1}{\sqrt{K}} + \frac{\delta_+ - \delta_-}{2\pi} \right)^2 + \frac{1}{2} \left(\frac{\delta_+ + \delta_-}{2\pi} \right)^2 - 1 \quad (\text{A.11})$$

where $\delta_{\pm} = 2\pi F_B(\pm q, \lambda)$ and K is the Luttinger parameter. Accordingly, one may numerically solve above integral equations to obtain $\mu_p(k)$ ($\mu_h(k)$). This exponent describes the power-law behavior of the DSF on the upper (lower) threshold, which dispersion is generated by adding 1-particle (1-hole) to the ground state, and thus the sign in Equation (A.9) is positive (negative). At first we solve the corresponding λ_p (λ_h) by using Equation (A.9), and then substitute this λ_p (λ_h) into the shift function $F_B(\mu|\lambda_p)$ ($F_B(\mu|\lambda_h)$). With the help of Equation (A.8), $\delta_{\pm}(k)$ is obtained, so is the exponent $\mu_p(k)$ ($\mu_h(k)$).

References

- [1] Pines D 1963 *Elementary Excitations in Solids* (W. A. Benjamin, New York)
- [2] Abrikosov A A, Gorkov L P and Dzyaloshinski I E 1963 *Methods of Quantum Field Theory in Statistical Physics* (Prentice Hall, Englewood Cliffs, New Jersey)
- [3] Francesco P, Mathieu P and Sénéchal D 2011 *Conformal Field Theory* (Springer-Verlag New York, Inc.)
- [4] Gogolin A O, Nersisyan A A and Tsvetlik A M 1998 *Bosonization and Strongly Correlated Systems* (Cambridge University Press, Cambridge)
- [5] Giamarchi T 2004 *Quantum Physics in One Dimension* (Oxford University Press, Oxford).
- [6] Cazalilla M A 2004 *J. Phys. B* **37** S1
- [7] Cazalilla M A, Citro R, Giamarchi T, Orignac E, and Rigol M 2011 *Rev. Mod. Phys.* **83** 1405
- [8] Imambekov A, Schmidt T L, and Glazman L I 2012 *Rev. Mod. Phys.* **84** 1253
- [9] Franchini F 2017 *An Introduction to Integrable Techniques for One-Dimensional Quantum Systems* (Springer, Cham)
- [10] Korepin V E, Bogoliubov N M, and Izergin A G 1993 *Quantum Inverse Scattering Method and Correlation Functions* (Cambridge University Press, Cambridge)
- [11] Schollwöck U. 2005 *Rev. Mod. Phys.* **77** 259
- [12] Lieb E H and Liniger W 1963 *Phys. Rev.* **130** 1605
Lieb E H 1963 *Phys. Rev.* **130** 1616
- [13] Girardeau M 1960 *J. Math. Phys.* **1** 516
Girardeau M 1965 *Phys. Rev.* **139** B500
- [14] Lenard A 1964 *J. Math. Phys.* **5** 930
Lenard A 1966 *J. Math. Phys.* **7** 1268
- [15] Vaidya H G and Tracy C A 1979 *Phys. Rev. Lett.* **42** 3
Vaidya H G and Tracy C A 1979 *J. Math. Phys.* **20** 2291

- [16] Pezer R and Buljan H 2007 *Phys. Rev. Lett.* **98** 240403
- [17] Settino J, Gullo N Lo, Plastina F, and Minguzzi A 2021 *Phys. Rev. Lett.* **126** 065301
- [18] Colcelli A, Viti J, Mussardo G, and Trombettoni A 2018 *Phys. Rev. A* **98** 063633
- [19] Colcelli A, Mussardo G, and Trombettoni A 2018 *Euro. Phys. Lett.* **122** 50006
- [20] Colcelli A, Defenu N, Mussardo G, and Trombettoni A 2020 *Phys. Rev. B* **102** 184510
- [21] Brand J and Cherny A Y 2005 *Phys. Rev. A* **72** 033619
- [22] Cherny A Y and Brand J 2006 *Phys. Rev. A* **73** 023612
- [23] Jiang Y-Z, Chen Y-Y, and Guan X-W 2015 *Chin. Phys. B* **24** 050311
- [24] Guan X-W and Batchelor M T 2011 *J. Phys. A* **44** 102001
- [25] De Nardis J, Wouters B, Brockmann M, and Caux J-S 2014 *Phys. Rev. A* **89** 033601
- [26] Buljan H, Pezer R, and Gasenzer T 2008 *Phys. Rev. Lett.* **100** 080406
- [27] Muth D and Fleischhauer M 2010 *Phys. Rev. Lett.* **105** 150403
Muth D, Schmidt B, and Fleischhauer M 2010 *New J. Phys.* **12** 083065
- [28] Iyer D and Andrei N 2012 *Phys. Rev. Lett.* **109** 115304
Iyer D, Guan H, and Andrei N 2013 *Phys. Rev. A* **87** 053628
- [29] Mossel J and Caux J-S 2012 *New J. Phys.* **14** 075006
- [30] Kormos M, Shashi A, Chou Y-Z, Caux J-S, and Imambekov A 2013 *Phys. Rev. B* **88** 205131
- [31] Kormos M, Collura M and Calabrese P 2014 *Phys. Rev. A* **89** 013609
- [32] Gangardt D M and Shlyapnikov G V 2003 *Phys. Rev. Lett.* **90** 010401
Gangardt D M and Shlyapnikov G V 2003 *New J. Phys.* **5** 79
Kheruntsyan K V, Gangardt D M, Drummond P D, and Shlyapnikov G V 2005 *Phys. Rev. A* **71** 053615
- [33] Nandani E J K P, Römer R A, Tan S-N, and Guan X-W 2016 *New J. Phys.* **18** 055014
- [34] Caux J-S and Calabrese P 2006 *Phys. Rev. A* **74** 031605(R)
- [35] Caux J-S, Calabrese P, and Slavnov N A 2007 *J. Stat. Mech.* P01008
- [36] Caux J-S 2009 *J. Math. Phys.* **50** 095214
- [37] Klerk A J J M, and Caux J-S 2023 arXiv: 2301.09224v1
- [38] Panfil M and Caux J-S 2014 *Phys. Rev. A* **89** 033605
- [39] Cheng S, Chen Y-Y, Guan X-W, Yang W-L, Mondaini R and Lin H-Q arXiv: 2209.15221
- [40] Cheng S, Chen Y-Y, Guan X-W, Yang W-L, and Lin H-Q, arXiv: 2211.00282v2
- [41] Granet E and Essler F H L 2020 *SciPost. Phys.* **9** 082
Granet E 2021 *J. Phys. A* **54** 154001
- [42] Xu W and Rigol M 2015 *Phys. Rev. A* **92** 063623
- [43] De Rosi G, Rota R, Astrakharchik G E and Boronat J 2022 *SciPost. Phys.* **13** 035
- [44] De Rosi G, Rota R, Astrakharchik G E and Boronat J arXiv: 2301.07626
- [45] Korepin V E 1982 *Commun. Math. Phys.* **86** 391
Korepin V E 1984 *Commun. Math. Phys.* **94** 93
- [46] Kojima T, Korepin V E, and Slavnov N A 1997 *Commun. Math. Phys.* **188** 657
- [47] Slavnov N A 1989 *Teor. Mat. Fiz.* **79** 232
Slavnov N A 1990 *Teor. Mat. Fiz.* **82** 389
- [48] Pitaevskii L and Stringari S 2016 *Bose-Einstein Condensation and Superfluidity* (Oxford University Press, Oxford)
- [49] See (I.5.24)-(I.5.27) of [10].
- [50] Imambekov A and Glazman L I 2008 *Phys. Rev. Lett.* **100** 206805
- [51] Imambekov A and Glazman L I 2009 *Phys. Rev. Lett.* **102** 126405
- [52] Kitanine N, Kozłowski K K, Maillet J M, Slavnov N A and Terras V 2012 *J. Stat. Mech.* P09001
- [53] Mahan G D 2000 *Many-Particle Physics* 3rd (Springer, New York)
- [54] Balents L 2000 *Phys. Rev. B* **61** 4429
- [55] Pustilnik M, Khodas M, Kamenev A, and Glazman L 2006 *Phys. Rev. Lett.* **96** 196405
- [56] Pereira R G, White S R, and Affleck I 2008 *Phys. Rev. Lett.* **100** 027206
- [57] Cheianov V V and Pustilnik M 2008 *Phys. Rev. Lett.* **100** 126403

- [58] Kamenev A and Glazman L I 2009 *Phys. Rev. A* **80** 011603
- [59] Schmidt T L, Imambekov A, and Glazman L I 2010 *Phys. Rev. Lett.* **104** 116403
- [60] For instance, see [36]: ‘Since the momentum is already sitting on a regular lattice, only the energy delta function is smoothened into a Gaussian. This has the unfortunate effect of blurring some would-be sharp excitation thresholds, but allows to obtain easily interpretable density plots of the DSF.’
- [61] Fabbri N, Clément D, Fallani L, Fort C and Inguscio M 2011 *Phys. Rev. A* **83** 031604(R)
Meinert F, Panfil M, Mark M J, Lauber K, Caux J-S, and Nägerl H C 2015 *Phys. Rev. Lett.* **115** 085301
Yang B, Chen Y-Y, Zheng Y-G, Sun H, Dai H-N, Guan X-W, Yuan Z-S, and Pan J-W 2017 *Phys. Rev. Lett.* **119** 165701
- [62] Guan X-W, Batchelor M T, and Lee C-H 2013 *Rev. Mod. Phys.* **85** 1633
- [63] Guan X-W and He P 2022 *Rep. Prog. Phys.* **85** 114001